



Original Article

Effect of dilution on micro hardness of Ni–Cr–B–Si alloy hardfaced on austenitic stainless steel plate for sodium-cooled fast reactor applications



S. Balaguru ^{a,*}, Vela Murali ^b, P. Chellapandi ^c, Manoj Gupta ^d

^a Vel Tech Rangarajan Dr. Sagunthala R&D Institute of Science and Technology, Chennai, India

^b College of Engineering, Guindy, Chennai, India

^c Indian Institute of Technology Madras, Chennai & Former CMD, BHAVINI, Kalpakkam, India

^d National University of Singapore, Singapore

ARTICLE INFO

Article history:

Received 22 May 2019

Received in revised form

3 August 2019

Accepted 18 August 2019

Available online 19 August 2019

Keywords:

Dilution

Hardness

Ni alloy

Austenitic stainless steel

Plasma transferred arc hardfacing (PTAH)

Travel speed

ABSTRACT

Many components in the assembly section of Sodium-cooled Fast Reactor are made of good corrosion-resistant 316 LN Stainless Steel material. To avoid self-welding of the components with the coolant sodium at elevated temperature, hardfacing is inevitable. Ni-based colmonoy-5 is used for hardfacing due to its lower dose rate by Plasma Transferred Arc process due to its low dilution. Since Ni–Cr–B–Si alloy becomes very fluidic while depositing, the major height of the weld overlay rests inside the groove. Hardfacing is also done over the plain surface where grooving is not possible. Therefore, grooved and un-grooved hardfaced specimens were prepared at different travel speeds. Fe content at every 100 μm of the weld overlay was studied by Energy Dispersive Spectroscopy and also the micro hardness was determined at those locations. A correlation between iron dilution from the base metal and the micro hardness was established. Therefore, if the Fe content of the weld overlay is known, the hardness at that location can be obtained using the correlation and vice-versa. A new correlation between micro hardness and dilution coefficient is obtained at different locations. A comparative study between those specimens is carried out to recommend the optimum travel speed for lower dilution.

© 2019 Korean Nuclear Society, Published by Elsevier Korea LLC. This is an open access article under the CC BY-NC-ND license (<http://creativecommons.org/licenses/by-nc-nd/4.0/>).

1. Introduction

Hardfacing is a type of surfacing in which a filler metal is deposited on to a surface or point of a metal to avoid galling and self-welding and also for providing resistance to wear or abrasion, impact etc [1,2]. Since the deposited metal is usually harder than the base metal, this process is known as hardfacing. Many components in nuclear reactor are made of 316 LN SS as the material has good corrosion resistance and high tensile strength. However, 316 LN SS is very ductile and hence hardfacing is inevitable to enhance the resistance to wear or abrasion, impact and galling and also to avoid self-welding of 316 LN SS with the hot liquid-metal sodium which acts as the coolant. Therefore, the service life of critical parts and assemblies can be extended [3,4]. Dilution is defined as the process when two metals are fusion-welded together by Tungsten

Inert Gas (TIG), Metal Inert Gas (MIG), Plasma Transferred Arc (PTA) or the submerged arc processes, then the final composition will consist of an admixture of the parent metal and the welding wire. In a Sodium-cooled Fast Reactor (SFR), when the 316 LN SS base metal is hardfaced by Ni–Cr–B–Si alloy, the elements from the base metal, mainly Fe, penetrate through the interface and dilute the weld overlay. Due to this, the hardness of the weld overlay gets affected. The reduction in hardness of the weld overlay depends upon the dilution percentage [5].

2. Literature review

Ni–Cr–B–Si alloy is available in powder form for the Plasma Transferred Arc Hardfacing (PTAH) and in rod form for the Gas Tungsten Arc Hardfacing (GTAH). When this alloy is hardfaced on 316 base metals, the dilution by Fe affects the hardness of the weld overlay because it suppresses the precipitation of primary chromium borides [6]. However, the dilution can be considerably minimized during PTAH by selecting suitable process variables

* Corresponding author.

E-mail address: iitmguru239@gmail.com (S. Balaguru).

when compared to GTAH process [7–9]. The presence of Cr_3C_2 , Cr_7C_3 and Cr_2B in γ nickel matrix from the XRD pattern of the powder provides hardness. A minimum dilution zone of about 1000 μm from the interface into the weld overlay can be obtained by the PTAH, which is much less than around 2.5 mm dilution zone obtained by GTAH [10,11]. The substrate dilution effect on hardness increases at higher temperature compared to that of room temperature due to softening of the material. Since the normal operating temperature of the SFR is 400 °C, the dilution study gains its importance [12,13]. Among all the hardfacing parameters, the travel speed is the most influencing parameter for controlling the dilution [14]. Therefore, this work aims at ascertaining the Fe dilution zone by preparing specimens from the lowest travel speed of 1.5 mm/s to the travel speed at which lack of fusion starts appearing without altering other hardfacing parameters during PTAH. A new approach which deals with the correlation between the micro hardness of the weld overlay and its dilution coefficient is obtained. From this correlation, if the hardness of the weld overlay at any particular height is measured, the dilution coefficient at that location can be ascertained.

3. Material selection

Most of the components of fast reactors including the grid plate assembly are made of 316LN SS as it has good resistance to corrosion due to smooth surface finish. It also has a high tensile strength of around 550 MPa and high temperature oxidation resistance [15,16]. This austenitic stainless steel has more amount of nickel (around 14%) than the duplex stainless steel. It has good weldability and prone to low erosion [17–20]. Therefore, it is taken as the base metal. Nickel based Ni–Cr–B–Si alloy is used for hardfacing due to its lower dose rate compared to Co based stellit-6 [21]. The precipitate of this alloy consists of 60% of chromium carbide and 20% chromium boride. The hardness of this alloy is mainly due to the chromium boride precipitate [22]. The chemical compositions 316LN SS and Ni–Cr–B–Si alloy are shown in Table 1 [23].

4. Specimen preparation

In the fast breeder reactors, Ni–Cr–B–Si alloy is not only deposited inside the annular groove of the bottom plate of grid plate, but also on the surface of the other 316 LN SS components like seal holder, seal rings, bushes, etc. [24,25]. Therefore, two types of specimens, namely (i) grooved (The alloy is deposited inside the groove of the base metal as it is fluidic in nature), (ii) un-grooved (The alloy is deposited on the surface of the base metal where the groove cannot be made), were prepared at the travel speeds of 1.5, 2, 2.5, 3 and 3.5 mm/s, respectively by PTAH. In this work, all the operating parameters were not optimized. The operating parameters were taken from the literature. These parameters are mentioned in Table 2 [10,23]. The travel speed which is the most influencing operating parameter to control dilution was not optimized by any researchers. Therefore, the travel speed was optimized based on lower dilution of Fe from the base metal into the weld overlay. Ni–Cr–B–Si powder was deposited in two layers with each layer of 2.5 mm. The preheating temperature for depositing the first layer is 400 °C. The dilution studies were carried out after the deposition of first layer as the penetration of Fe from

Table 2
Hardfacing parameters maintained in PTAH process [10,23].

Technology	Parameter
Current	150 A
Voltage	24 V
Polarity	DC
Shielding gas	Argon
Powder feed rate	30 g/min
Shielding gas flow rate	12 L/min
Travel speeds	1.5, 2, 2.5, 3 and 3.5 mm/s
Medium of cooling	Vermiculate powder

the base metal takes place into the first layer. The specimens were slowly cooled to room temperature by inserting them into vermiculate powder to avoid cracking. The second layer was deposited after the dilution and micro hardness studies, conveniently after two weeks, for the future work. Therefore, the total height of the deposit reached to 5 mm. In order to maintain the height of weld overlay as 4 mm, as carried out in SFR, the additional 1 mm of the deposit is machined to get evenness from both the types of specimens. The preheating temperature for depositing the second layer is 500 °C. The preheating temperature for the second layer is higher as it is done over the first layer which is brittle. In case of grooved specimens, the width of the groove was reduced from 50 mm to 20 mm and the angle of the groove was increased from 30° to 45° to achieve a crack-free deposit [26]. Three specimens at each travel speed in both the grooved and un-grooved types were prepared. The geometry of grooved specimens represents the cross section of the annular portion of the bottom plate of hardfaced grid plate and is shown in Fig. 1(a). All the specimens were polished and etched with Oxalic acid. The geometry of the un-grooved specimens is same as that of the grooved specimens for comparison and is shown in Fig. 1(b). Fig. 2(a) and (b) show the cut-sections of defect-free grooved and un-grooved (machined at the top) samples respectively after the deposition of second layer. The unwanted portion of base metal was removed from these figures.

5. Results and discussion

All the grooved and un-grooved specimens were inspected by radiography using Ir-192 Industrial Radiography System to predict whether there was any defect. No hardfacing defect was noticed in both grooved and un-grooved specimens prepared up to the travel speed of 3 mm/s. One out of 3 of the grooved specimens and two out of 3 of the un-grooved specimens hardfaced at the travel speed of 3.5 mm/s had lack of fusion. In order to still converge the study, three specimens in both grooved and un-grooved types were prepared at the intermediate travel speed of 3.25 mm/s. One out of three specimens, in both un-grooved and grooved type, had small level of lack of fusion. This represents that the maximum travel speed for defect-free deposit as 3 mm/s. Therefore, the specimens prepared up to 3 mm/s were considered for metallurgical investigations in both the types. Fig. 3(a) shows the radiographic image of defect-free un-grooved specimen at the travel speed of 2.5 mm/s. Fig. 3(b) shows the lack of fusion in the grooved specimen at the travel speed of 3.25 mm/s. The specifications of Ir-192 Industrial Radiography System are shown in Table 3.

Table 1
Chemical composition of 316 SS LN and colmonoy-5 [23].

Material	C	Mn	Si	P	S	Cr	Mo	Ni	N	Fe	B
316 LNSS (Base metal)	0.03	2.0	0.75	0.045	0.03	18	3.0	14	0.14	62.05(As Bal)	–
Ni–Cr–B–Si (colmonoy-5 powder)	0.6	0.1	3.8	–	–	11.5	–	77 (As Bal)	–	4.4	2.6

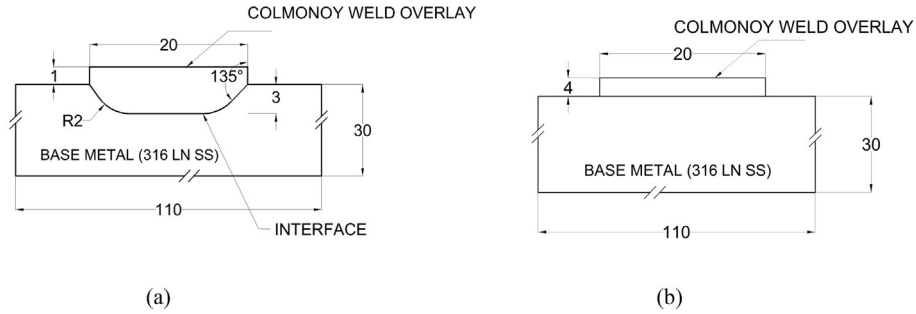


Fig. 1. Geometries of (a) grooved and (b) un-grooved specimens.

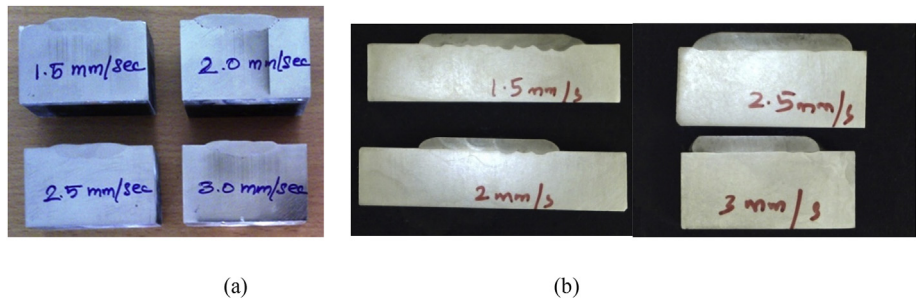


Fig. 2. Cut-sections of defect-free (a) Grooved specimens as deposited (b) Un-grooved specimens as machined.

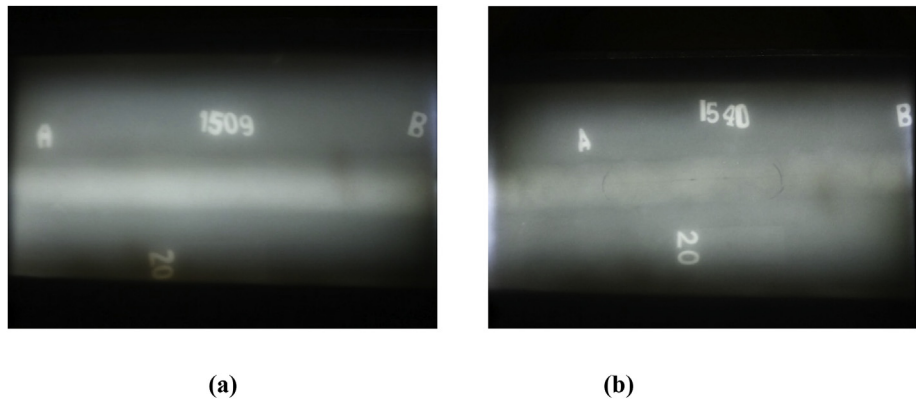


Fig. 3. (a) Defect-free un-grooved specimen at the travel speed of 2.5 mm/s (b) Grooved specimen with lack of fusion at the travel speed of 3.25 mm/s.

5.1. Estimation of average dilution

Before going in for the detailed analysis, the average dilution was determined for different travel speeds to narrow down the study. The macro images of the welded cross-section were captured by Dewinter Image analysis software in the area mode and average dilution (%) was determined after depositing the first layer using the formula mentioned in Fig. 4(a) [27,28]. Fig. 4(b) shows the dilutions of the grooved and un-grooved specimens on the basis of

mean of areas taken in three locations of set-1 specimens. The geometry of the set-1 specimens are shown in Fig. 1. The set-1 specimens are shown in Fig. 2. The variations in average dilution % obtained from other two specimens of the same travel speed lies between 0.5 and 1.5%. Therefore, a set (known as set-1) comprising one specimen from each travel speed is considered for further investigations under both grooved and un-grooved types separately.

Table 3 Specifications of Ir-192 industrial radiography system.

Technology	Parameter
Shield	Depleted Uranium 37 lbs. (17 kg) with durable titanium S-tube
Rated Capacity	150 Ci of IR-192 and SE-75 (125ci + 20%); 5500 Gbq
Sources	SPEC Model G-60 source assembly.
Dimensions	14.5”L × 5.375”W × 5.5625”H

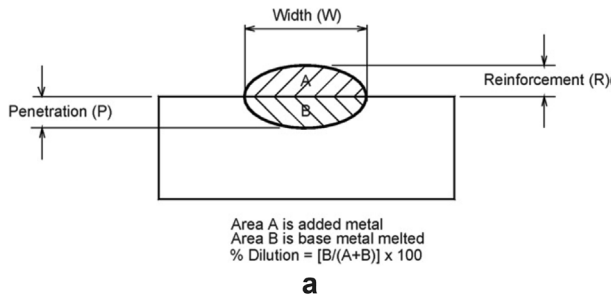


Fig. 4a. Representation of the average Dilution.

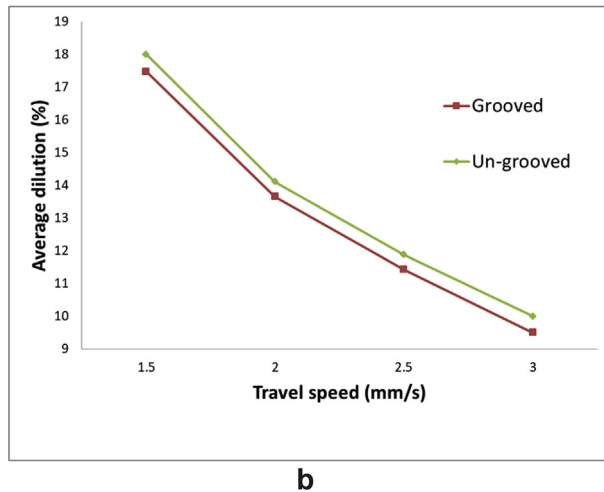


Fig. 4b. Variation in average Dilution for different travel speeds.

5.2. Determination of Fe dilution % from the base metal

From Fig. 4(b), it is found that the average dilution decreases as the travel speed increases in both the grooved and un-grooved specimens due to rapid solidification of the molten alloy. Moreover, the dilution changes as the distance from the interface into the weld overlay also changes. Due to dilution, the composition of the weld overlay gets changed and hence its properties too. To study in detail, the EDS results were taken in the transverse direction starting from the interface into the weld overlay in every 100 μm step to predict the extent of Fe penetration from the base metal. Micro hardness of the weld overlay at those locations was determined by Vickers Hardness Tester. The penetration of Fe into the weld overlay affects the hardness of the weld overlay. Three readings were taken along the same axis from the interface and the mean of them was taken as the chemical composition. Fig. 5(a) shows the Supra 55 Scanning Electron Microscope with EDS attachment, needed for the investigation. Fig. 5(b) and (c) represent the SEM micrograph and the EDS results of grooved for the travel speed of 2 mm/s taken at the height of 500 μm above the interface. Fig. 5(d) and (e) represent the SEM micrograph and the EDS results of un-grooved for the same travel speed of 2 mm/s taken at the height of 500 μm above the interface. Table 4 shows the specifications of the Supra 55-SEM used for characterization. Table 4 also contains the specifications of the Micro Vickers Hardness Tester used for the estimation of micro hardness at various locations of the specimens.

From the weight % of Fe content, the iron dilution from the base metal into the deposit can be determined. From Table 1, an

elemental dilution formula to determine iron dilution can be devised from the final composition of the weld metal, using the EDS results.

Let x = Iron dilution % from the base metal. Eg For 40%, $x = 0.4$
 $(1-x)$ = Iron dilution % from the weld overlay. Eg. If $x = 0.4$, then $(1-x) = 0.6$
 V = % of iron in the final weld composition

Base metal 316 LN SS has 62.05% of Fe element and hardfacing alloy colmonoy-5 has 4.4% of Fe element. The Fe element from the base metal and the Fe element from the molten colmonoy by the PTAH process contribute to the Fe content in the final weld composition in the diluted region. This study focuses up to the diluted region of the weld overlay. Therefore, if 10% of 62.05 of Fe from the base metal goes into the diluted region, the remaining 90% of 4.4 of Fe is contributed by the molten colmonoy by the PTAH process. These two contributions lead to the Fe content in the final solidified weld composition of diluted region.

$$\text{Therefore, } x \times 62.05 + (1 - x) 4.4 = V \quad \text{or} \quad x = \frac{V - 4.4}{57.65} \quad (1)$$

Multiplying x by 100, iron dilution % can be obtained.

Fig. 6(a) shows the hardness distribution across the interface in the diluted region of the weld overlay for the travel speed of (a) 2 mm/s (b) 3 mm/s respectively. From the graphs, it is seen that the diluted region for grooved specimen is nearly 100–200 μm shorter than that of the un-grooved specimen for the same travel speed due to early attainment of maximum hardness.

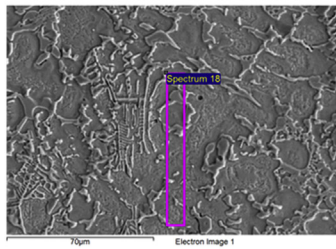
5.3. Relationship between Fe dilution from the base metal and the hardness of the weld overlay

This overall Fe content identified by the EDS results at each location of the final solidified weld composition is the sum of Fe content penetrated from the base metal in to the weld overlay and its own Fe content contributed by the molten colmonoy by the PTAH process at that location. Out of these two components of Fe contents at each location, the Fe content penetrated from the base metal is responsible for the reduction in hardness of the weld overlay. Therefore, Fe dilution (%) is obtained from the % of Fe in the weld composition using Eqn (1) and compared with the reduction in hardness at that location. Fig. 7 shows the variation in Fe content of the grooved specimens over the region where the hardness of both the base metal and the weld overlay got affected, by taking the mean of three readings along the same axis.

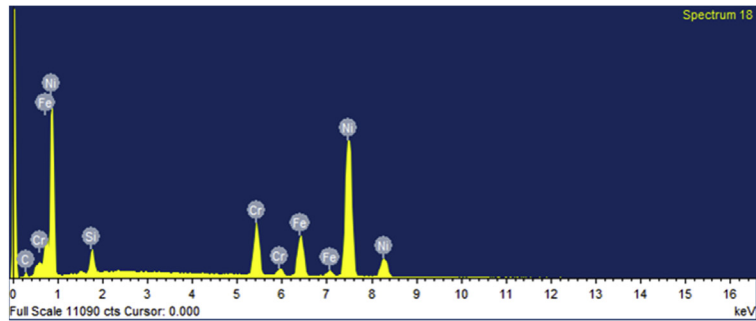
From the EDS results shown in Fig. 5(c), Fe content in the final weld composition is found to be 11.94% for grooved specimen. From Eqn (1), for this 11.94% of Fe content, the Fe dilution from the base metal is 13% which is responsible for the reduction in hardness. This 13% Fe dilution from the base metal (excluding the Fe present in the powder) reduces the hardness of the weld overlay from 465 to 290.7 VHN, amounting to a loss of 37.5%. Therefore, the ratio of reduction in hardness to Fe dilution % from the base metal for this travel speed of 2 mm/s is around 2.88 for grooved specimen. Similarly, at the height of 800 μm from the interface, Fe content in the final weld composition is found to be 10.58% for grooved specimen. From Eqn (1), for this 10.58% of Fe content, the Fe dilution from the base metal is 10.7% which is responsible for the reduction in hardness. This 10.7% Fe dilution from the base metal (excluding the Fe present in the colmonoy powder) reduces the hardness of the weld overlay from 465 to 366 VHN, amounting to a loss of 21.3%. Therefore, the ratio of reduction in hardness to Fe



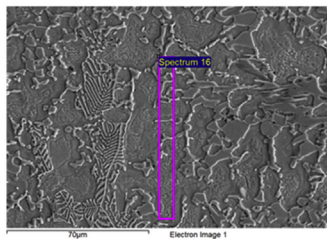
(a)



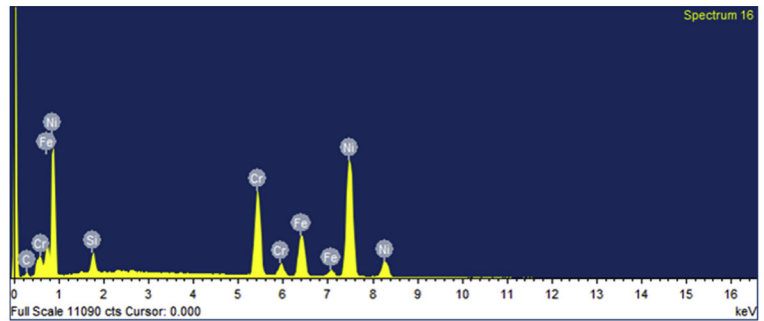
(b)



(c)



(d)



(e)

Fig. 5. (a) Supra 55-Scanning Electron Microscope with EDS attachment. Fig. 5(b) and (c) Micrograph and EDS results at a height of 500 µm above the interface of grooved specimen. Fig. 5 (d) and (e) Micrograph and EDS results at a height of 500 µm above the interface of un-grooved specimen.

Table 4

Specifications of the supra 55-SEM and micro vickers hardness tester.

Supra 55-Scanning Electron Microscope with EDS attachment	Micro Vickers Hardness Tester
Resolution: 1 nm at 15 kV, 4 nm at 0.1 kV	Make: Wilson Wolpert – Germany
Magnification 12–900,000 X	Testing load rang: 10 g to 1 kg Load
Accelerating voltage: 0.1–30 kV	Vernier caliper least count: 0.01 mm
Variable pressure: 2–133 Pa	Hardness testing Scale: HV, HRA, HRC, 15 N, 30 N

dilution % from the base metal for this travel speed of 2 mm/s is around 2 for grooved specimen. Using the ratios obtained at 500 µm and 800 µm, the hardness at any location between them (say 700 µm) can be obtained by the following empirical relation:

Fe content at the location of 700 µm as per EDS survey = 10.41%

Corresponding Fe dilution from the base metal as per Eqn (1) = 10.43%

The ratio of hardness reduction % and Fe dilution % from the base metal at 700 µm can be obtained by interpolating the corresponding values of 500 µm and 800 µm as follows:

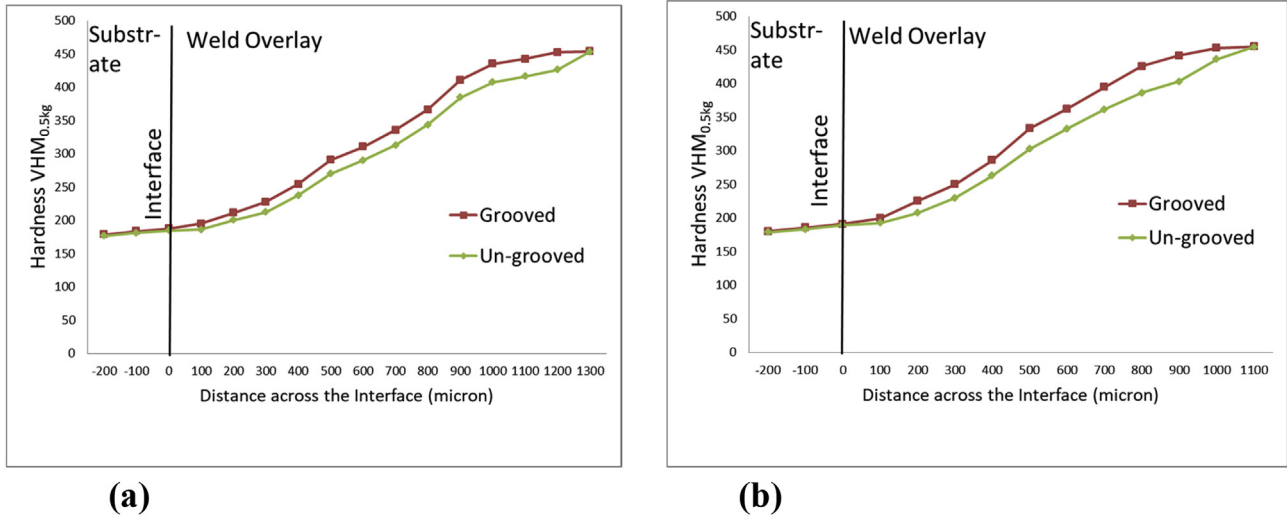


Fig. 6. Hardness distribution across the interface in the diluted region of the weld overlay for the travel speed of (a) 2 mm/s (b) 3 mm/s.

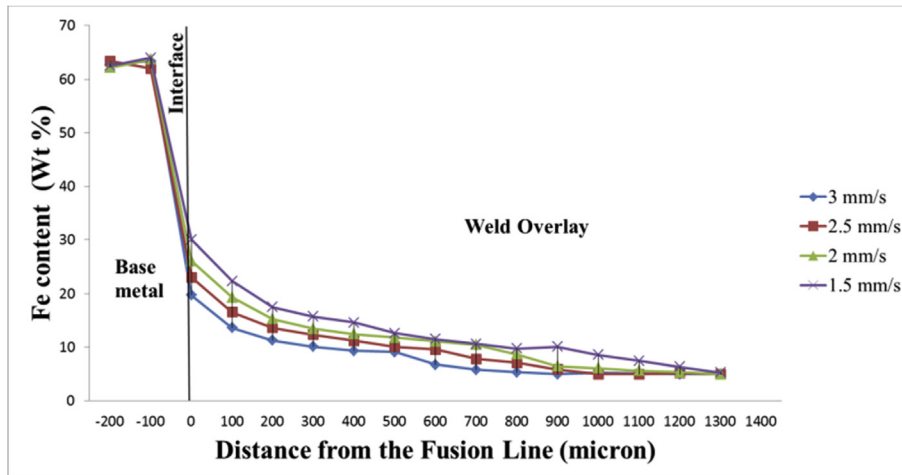


Fig. 7. Variation in Fe content of grooved specimens over the hardness-affected region.

$$x - 2 = \frac{2.88 - 2}{800 - 500} (700 - 500)$$

$$x = 2.587$$

$$\frac{\text{Reduction in hardness \%}}{\text{Fe dilution \% from the base metal}} = 2.587$$

$$\frac{\text{Reduction in hardness \%}}{10.43} = 2.587$$

$$\text{Reduction in hardness \%} = 27$$

$$\text{Hardness at the location} = 73 \% \text{ of Surface Hardness}$$

$$= 0.73 \times 465 = 339 \text{ VHN}$$

from the micro hardness survey, the hardness at that location of the grooved specimen for the travel speed of 2 mm/s is found to be 336 VHN. The same analogy can be applied to grooved as well as un-

grooved specimens of all the defect-free travel speeds.

5.4. Relationship between the dilution coefficient and the hardness of the weld overlay

The effect of dilution coefficient on the hardness of the weld overlay is studied using the hardness values obtained already. The relationship between the hardness of the weld overlay and the dilution coefficient is given by the following equation:

$$\Delta H = \Delta H_0 e^{-\beta \zeta} \tag{2}$$

where,

$$\beta = \text{Dilution coefficient}$$

$$\zeta = \frac{y_c}{y_0} = \frac{\text{Total distance of the location from the base metal where the hardness got affected}}{\text{Total distance of the hardness affected region}}$$

$$\zeta = \frac{\text{Distance of the location from the interface into weld overlay} + \text{Distance upto which the hardness got affected into the base metal from the interface}}{\text{Distance upto which the hardness got affected into the base metal from the interface} + \text{Hardness affected region of the weld overlay}}$$

for example, the hardness of the base metal got influenced up to 200 μm below the interface for all the travel speeds. Therefore, for the travel speed of 2 mm/s of grooved type, the value of ζ at the interface is calculated as follows:

$$\zeta = \frac{y + 200}{200 + 1000} = \frac{0 + 200}{200 + 1000} = 0.167$$

where y is the distance of the location of the weld overlay from the interface.

ΔH = Hardness at the height of y – Hardness of the base metal At the interface, y = 0. Therefore, $\Delta H = 183.4 - 175 = 8.4$ VHN
 ΔH_0 = Hardness of the surface of the deposit – Hardness of the base metal = 465 – 175 = 290 VHN
 where, 465 VHN = Hardness of the surface of the deposit at the end of 1st layer (un-diluted hardness).

Using Eqn (2), dilution coefficients have been determined for different travel speeds of grooved and un-grooved specimens from the interface in every 250 μm as represented in Fig. 8(a) and (b) respectively.

From Fig. 8(a) and (b), it is seen that dilution coefficient decreases from the interface into the weld overlay for both grooved and un-grooved specimens and reaches the value close to zero where the dilution region ends for the different travel speeds of PTAH. By magnifying the bottom portion of the above graphs, the end of dilution region for the different travel speeds can be ascertained for both grooved and un-grooved specimens. At any particular location in the weld overlay, as the travel speed increases, the dilution coefficient decreases due to faster solidification. When the dilution coefficient is 19.16 at the interface for

2 mm/s of grooved specimen, the reduction in hardness is found to be 60% as compared to surface hardness. When the dilution coefficient decreases to 5.16, 1.64 and 0.75 at 250 μm, 500 μm and 750 μm respectively, the reduction in hardness is found to be 53%, 37.5% and 26.8% respectively. When the dilution coefficient decreases, the percentage hardness reduction of the weld overlay also decreases. Moreover, a small reduction in dilution coefficient causes a significant reduction in hardness (%) after 250 μm from the weld overlay till the diluted region. It shows that the hardness is increasing slowly up to 250 μm and hence the sufficient ductility is maintained near the interface to avoid de-bonding for all the travel speeds of both the types of specimens.

6. Conclusions

The following qualitative and quantitative conclusions have been arrived at:

Qualitative Conclusions: These qualitative conclusions will fulfill the following societal needs:

- This study addresses the complex subject relevance to the hardfacing of power plant components.
- These investigations provide a vital input for hardfacing NiCrBSi alloy on the austenitic components used in the SFR to attain required hardness in the shortest height.
- A new approach has been established to find the dilution coefficient which represents the extent of micro hardness of the weld overlay diluted. If the dilution coefficient at any location in the weld overlay is known, its hardness at that location can be determined and vice-versa. Therefore, it would be possible to maintain the required hardness at that location.

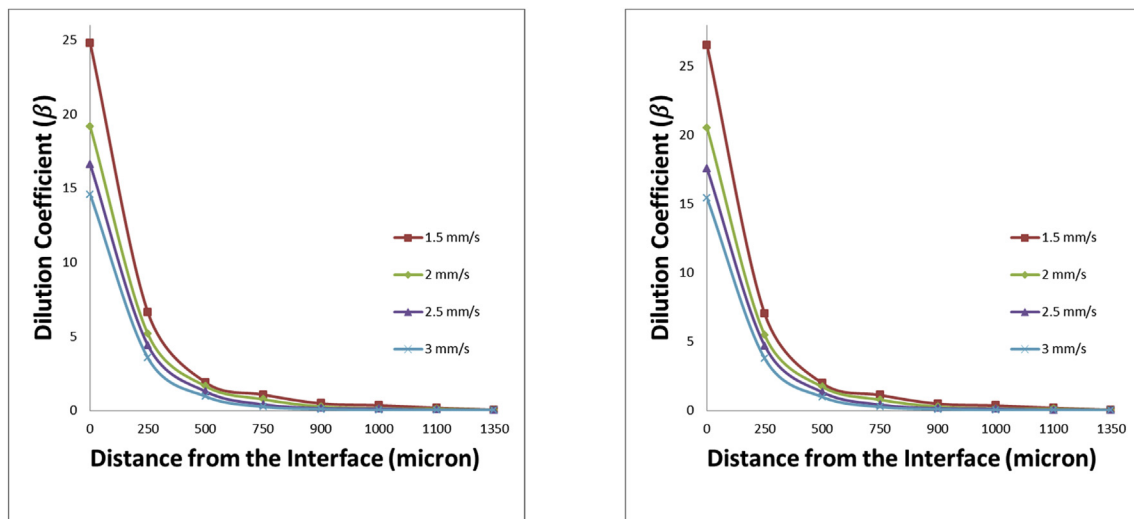


Fig. 8. Variation of Dilution coefficients at different locations from the interface into weld overlay of (a) grooved specimen (b) un-grooved specimen.

Quantitative Conclusions

- By optimizing the travel speed of the PTA hardfacing to 3 mm/s, the hardness gets increased by 2.65 times that of the base metal within the height of around 700–750 μm for both grooved and un-grooved specimens.
- The average dilution is found to be as low as 9.4% and 10.05% respectively for grooved and un-grooved specimens for the travel speed of 3 mm/s.
- A correlation between iron dilution from the base metal and the hardness of the weld overlay is established. Therefore, if the Fe content of the weld overlay is known by EDS at a location, the hardness at that location can be obtained using the correlation and vice-versa.
- The dilution coefficient plays a major role only after 250 μm from the interface into the weld overlay as a small reduction in value causes considerable increase in hardness value of the weld overlay.
- The increase in travel speed from 1.5 mm/s to 3 mm/s causes only a rise of 7–8 VHN at the interface whereas the maximum hardness of 465 VHN was attained at the height of 700–750 μm , compared to more than 1000 μm for 1.5 mm/s. Hence the ductility is also maintained at the interface to avoid de-bonding as well as maximum hardness is attained at a shorter height for the travel speed of 3 mm/s for both grooved and un-grooved types. Hence the travel speed of 3 mm/s is recommended for the PTA hardfacing for both grooved and un-grooved specimens keeping other parameters in Table 2 unaltered.

References

- [1] R.S. Parmar, *Welding Processes and Technology*, second ed., Khanna Publishers, New Delhi, 2003.
- [2] Hemant Kumar, V. Ramakrishnan, S.K. Albert, A.K. Bhaduri, K.K. Ray, Self-welding susceptibility of NiCrB hardfaced weld overlay with and without NiCrB weld overlay on 316LN stainless steel in flowing sodium at elevated temperature, *J. Nucl. Mater.* 484 (2017) 141–147.
- [3] A.C. Davies, *Welding*, tenth ed., Cambridge University Press, Cambridge, 1996.
- [4] A.S. Shahi, Sunil Pandey, Modelling of the effects of welding conditions on dilution of stainless steel claddings produced by gas metal arc welding procedures, *J. Mater. Process. Technol.* 196 (2008) 339–344.
- [5] S. Balaguru, K. Deenadayalan, Murali Vela, P. Chellapandi, Influence of welding speed over dilution for circular grid plate hardfaced with colmonoy-5, *Appl. Mech. Mater.* 565 (2014) 53–58.
- [6] I. Hemmati, V. Ocelik, Th. JM. De Hosson, Dilution effects in laser cladding of Ni-Cr-B-Si-C hardfacing alloys, *Mater. Lett.* 84 (2012) 69–72.
- [7] C.R. Das, S.K. Albert, A.K. Bhaduri, G. Kempulraj, A novel procedure for fabrication of wear resistant bushes for high temperature application, *J. Mater. Process. Technol.* 141 (2003) 60–66.
- [8] Byoung Hyun Yoon, Yong Soo Ahn, Lee Chang, The effect of dilution on HAZ liquation cracking in PTA Ni-base superalloys overlay deposit, *ISIJ Int.* 42 (2002) 178–183.
- [9] K. Siva, N. Murugan, A study on the influence of PTA process parameters on pitting corrosion resistance of nickel based overlays, *Procedia Eng* 64 (2013) 1147–1156.
- [10] C. Sudha, P. Shankar, R.V. Subba Rao, R. Thirumurugesan, M. Vijayalakshmi, Baldev Raj, Microchemical and microstructural studies in a PTA weld overlay of Ni–Cr–Si–B alloy on AISI304L stainless steel, *Surf. Weld overlays Technol.* 202 (2008) 2103–2112.
- [11] V. Balasubramanian, A.K. Lakshminarayannan, R. Varahamoorthy, S. Babu, Application of response surface methodology to prediction of dilution in plasma Transferred Arc hardfacing of stainless steel on carbon steel, *J. Iron Steel Res. Int.* 16 (2009) 44–53.
- [12] C.R. Das, S.K. Albert, A.K. Bhaduri, G. Kempulraj, A novel procedure for fabrication of wear resistant bushes for high temperature application, *J. Mater. Process. Technol.* 141 (2003) 60–66.
- [13] P. Chellapandi, P. Puthiyavinayagam, V. Balasubramaniyam, S. Raghupathy, V. Rajan Babu, S.C. Chetal, Baldev raj, development of innovative reactor assembly components towards commercialization of future FBRs, *Energy Procedia* 7 (2011) 359–366.
- [14] V. Balasubramanian, A.K. Lakshminarayannan, R. Varahamoorthy, S. Babu, Understanding the parameters controlling plasma transferred arc hardfacing using response surface methodology, *Mater. Manuf. Process.* 23 (2008) 1–9.
- [15] S. Ramesh, Prabu Rajendran, N. Elango, Experimental investigation of structure, wear, and erosion resistance of SS316 substrate coated with TiC–Al₂O₃ composite by laser cladding, *High Temp. Mater. Process.* 22 (2018) 63–71.
- [16] P. Suresh, R. Venkatesan, T. Sekar, N. Elango, V. Sathiyamoorthy, Optimization of intervening variables in MicroEDM of SS 316L using a genetic algorithm and response-surface methodology, *Strojnicki Vestnik/J. Mech. Eng.* 60 (2014) 656–664.
- [17] Q.B. Nguyen, V.B. Nguyen, C.Y.H. Lim, Q.T. Trinh, S. Sankaranarayanan, Y.W. Zhang, M. Gupta, Effect of impact angle and testing time on erosion of stainless steel at higher velocities, *Wear* 321 (2014) 87–93.
- [18] A.K. Bhaduri, R. Indira, S.K. Albert, B.P.S. Rao, S.C. Jain, S. Asokkumar, Selection of hardfacing material for components of the Indian prototype fast breeder, *J. Nucl. Mater.* 334 (2004) 109–114.
- [19] S.C. Chetal, V. Balasubramaniyam, P. Chellapandi, P. Mohanakrishnan, P. Puthiyavinayagam, C.P. Pillai, S. Raghupathy, T.K. Shanmugham, C. Sivathanu Pillai, The design of the prototype fast breeder reactor, *Nucl. Eng. Des.* 236 (2006) 852–860.
- [20] Q.B. Nguyen, C.Y.H. Lim, V.B. Nguyen, Y.M. Wan, B. Nai, Y.W. Zhang, M. Gupta, Slurry erosion characteristics and erosion mechanisms of stainless steel, *Tribol. Int.* 79 (2014) 1–7.
- [21] D. Kesavan, M. Kamaraj, The microstructure and high temperature wear performance of a nickel base hardfacedweld overlay, *Wear* 204 (2010) 4034–4043.
- [22] D. Kesavan, M. Kamaraj, Influence of aging treatment on microstructure, wear and corrosion behavior of a nickel base hardfaced weld overlays, *Wear* 272 (2011) 7–17.
- [23] S. Balaguru, Murali Vela, P. Chellapandi, Effects of different operating temperatures on the tensile properties of the grid plate hardfaced with colmonoy in a pool type sodium-cooled fast reactor, *Sci. Technol. Nucl. Install.* (2017) 1–9, 2017.
- [24] Baldev Raj, Materials science research for sodium cooled fast reactors, *Bull. Mater. Sci.* 32 (2009) 271–283.
- [25] Baldev Raj, Materials and manufacturing technologies for sodium cooled fast reactors and associated fuel cycle: innovations and maturity, *Energy Procedia* 7 (2011) 186–198.
- [26] S. Balaguru, Murali Vela, P. Chellapandi, Effects of welding speeds on macro and microstructures in hardfacing of colmonoy on un-grooved and grooved 316 L(N) SS base metal, *Int. J. Appl. Eng. Res.* 10 (2015) 25627–25631.
- [27] N. Murugan, R.S. Parmar, S.K. Sud, Effect of submerged arc process variables on dilution and bead geometry in single wire surfacing, *J. Mater. Process. Technol.* 37 (1993) 767–780.
- [28] N. Murugan, R.S. Parmar, Mathematical models for bead geometry prediction in automatic stainless steel surfacing by MIG welding, *Int. J. Join. Mater.* 7 (1995) 71–80.